

Micro-patterned porous silicon using proton beam writing

M. B. H. Breese, D. Mangaiyarkarasi, E. J. Teo*,
A. A. Bettiol and D. Blackwood*

*Centre for Ion Beam Applications, Department of Physics,
National University of Singapore, Singapore 117542*

**Materials Science and Engineering Department, National University of Singapore, Singapore 117542*

Abstract. A high-energy beam of hydrogen or helium ions focused to a small spot in a nuclear microprobe selectively damages a silicon lattice. This damage acts as an electrical barrier during subsequent formation of porous silicon by electrochemical etching of p-type wafers, so the un-irradiated regions are preferentially anodized. This process has opened up new research directions for the fabrication of a variety of high-aspect ratio, multi-level microstructures in silicon, such as gratings, photonic lattices and waveguides. The same process enables local modifications and control of the properties of the porous silicon, leading to new luminescent micro-structures in which both the spatial location and the wavelength and intensity of emission can be carefully controlled. The reflectivity and transmission of Bragg reflectors and microcavities fabricated in porous silicon can also be controlled using this same process and examples are given of each of these applications.

INTRODUCTION

Porous silicon (PSi) is of interest due to its photoluminescence and electroluminescence properties [1,2], raising the possibility of producing light emitting devices made of PSi and microelectronics compatibility. A potentially important application of PSi is the production of combined optical/electronic devices incorporating patterned porous material directly onto a single-crystal Si substrate with a high spatial resolution. The photoluminescence from PSi can be greatly improved by placing it in a Fabry-Perot microcavity with dimensions comparable to the optical emission wavelength. One dimensional photonic structures based on alternating high and low porosity PSi layers have found applications as dielectric mirrors in the form of Distributed Bragg Reflectors [3], microcavities [4,5] and waveguides [6]. PSi exhibits optical properties consistent with a single effective refractive index despite its nanoscale structural inhomogeneity. The refractive index of PSi is lower than for bulk silicon; it is inversely

proportional to the etch current density used for anodisation. A Distributed Bragg Reflector selectively reflects a band of incident wavelengths and is formed in PSi by periodically lowering and raising the etch current density, resulting in a sequence of porous layers with alternating high and low refractive index. Highly-doped p-type silicon ($\sim 0.01 \Omega\text{.cm}$) is commonly used to fabricate such PSi-based photonic structures because a wide range of refractive index can be achieved.

Many new technologies require the fabrication of precise three-dimensional structures in silicon [7,8]. One major limitation of conventional lithography and silicon etching technologies for these applications is the multiple processing steps involved in fabricating free-standing multilevel structures. Electrochemical etching of silicon in hydrofluoric acid is emerging as an alternative technique for micromachining due to its low cost, fast etching process and easy implementation. The

porous silicon produced can be easily removed by immersion in a potassium hydroxide (KOH) solution.

ION IRRADIATED POROUS SILICON

Figure 1 shows the basis of producing micro-patterned silicon surfaces, controlled photoluminescence from bulk P*Si* and controlled reflectivity from P*Si* Bragg reflectors. A finely-focused beam of MeV ions is scanned over the wafer surface using a nuclear microprobe [9], in this case at the National University of Singapore, which can focus MeV ion beams to spot sizes of less than 50 nm [10]. The ion beam loses energy as it penetrates the semiconductor and comes to rest at a well-defined range, equal to $\sim 8 \mu\text{m}$ for 2 MeV helium ions, and $\sim 50 \mu\text{m}$ for 2 MeV protons in silicon. The stopping process causes the silicon crystal to be damaged, by producing additional vacancies in the semiconductor. A higher beam fluence at any region produces a higher vacancy concentration, so by pausing the focused beam for different amounts of time at different locations, any pattern of localized damage can be built up.

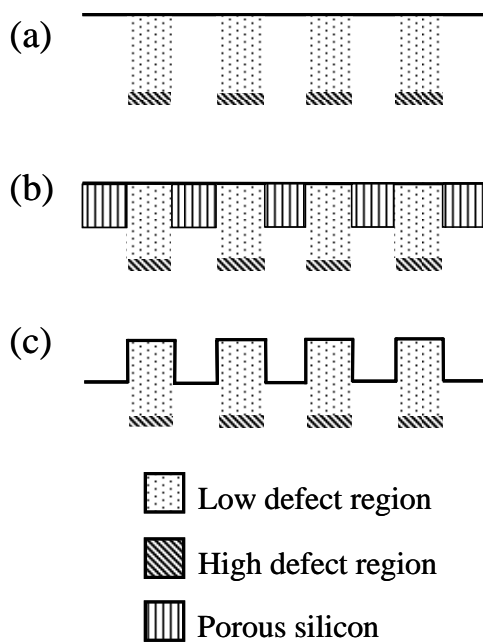


FIGURE 1. (a) Patterning of *p*-type silicon with proton beam writing, (b) electrochemical etching to selectively form patterned porous silicon and (c) removal of porous silicon with dilute KOH solution to form a micromachined structure

The irradiated wafer is then electrochemically etched in a dilute solution of hydrogen fluoride. An electrical current is passed through the wafer which causes the formation of porous silicon at the surface. The buried regions of high vacancy concentration inhibit this formation process, so a thinner layer of porous silicon is produced at the irradiated regions. A very large beam dose may reduce the etch rate to zero at the irradiated regions. The etched sample comprises patterned areas of porous silicon which may emit light with greater or lesser intensity, or different wavelength, compared with the surrounding unirradiated regions. If the anodisation is repeated with alternating low and high current densities then the range of wavelengths of incident light which are reflected from the resultant Bragg reflector depends on the ion irradiation dose. If the etched sample is immersed in KOH, the porous silicon is removed, leaving the final patterned structure on the wafer surface as a three-dimensional representation of the scanned pattern area and fluence.

MICROMACHINING RESULTS

Recent results on fabricating high-aspect ratio, multilevel structures in silicon have been published in Refs. [11-13]. Fig. 2a,b shows Scanning Electron Microscope (SEM) images of a linear waveguide with a grating at the top surface with a $1 \mu\text{m}$ period. This is designed to selectively transmit at certain infra-red wavelengths along the waveguide while the grating modifies which wavelengths are transmitted, depending on the periodicity. This waveguide was formed by first fabricating the waveguide using the above micromachining process, then spinning on a layer of polymer resist and creating the grating in the polymer using a second irradiation with a beam spot focused to 100 nm or less [14]. The pattern was then transferred to the silicon waveguide top surface using reactive ion etching.

After etching beyond the end of range, the isotropic electrochemical etching process starts to undercut the irradiated structure, so multi-level micromachined structures can be created by irradiating with two different proton energies. The regions irradiated with lower energy become undercut at a shallower etch depth while regions irradiated with higher energy protons continue to increase in height. In this way, multi-level free-standing microstructures can be fabricated in a single etch step. To demonstrate this capability, bridge structures were irradiated with 0.5 MeV protons (range $\sim 6 \mu\text{m}$), and supporting pillars with 2 MeV protons

(range $\sim 48 \mu\text{m}$). Fig. 2c shows the resultant ‘StoneHenge’ structure after prolonged etching. The bridges are fully undercut and separated from the substrate. They remain supported by the pillars irradiated by higher energy.

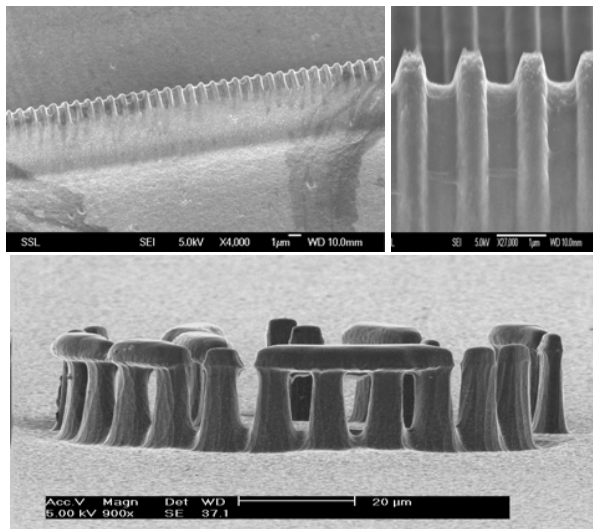


FIGURE 2. SEM images of (a) linear waveguide with a grating at the top surface with a $1 \mu\text{m}$ period, (b) higher magnification. (c) micromachined ‘StoneHenge’ structure, 100 microns in diameter.

PATTERNED POROUS SILICON RESULTS

We have undertaken a comprehensive study of the effects of ion irradiation on a wide range of different resistivity *p*-type wafers, and recorded the resultant photoluminescence intensity and wavelength [15-18]. Three different resistivity *p*-type silicon wafers were patterned with a focused beam of 2 MeV helium ions. After irradiation the wafers were anodized, producing a porous layer several microns in thickness. Fig. 3 plots the measured photoluminescence intensity and peak wavelength emission as a function of ion dose. There are two resistivity regimes in *p*-type silicon where photoluminescence is affected in different ways by ion irradiation: for low resistivity ($\sim 0.01 \Omega\cdot\text{cm}$) wafers irradiation primarily results in a large PL increase whereas for moderate resistivity ($0.1-10 \Omega\cdot\text{cm}$) wafers irradiation primarily results in a large PL wavelength red-shift.

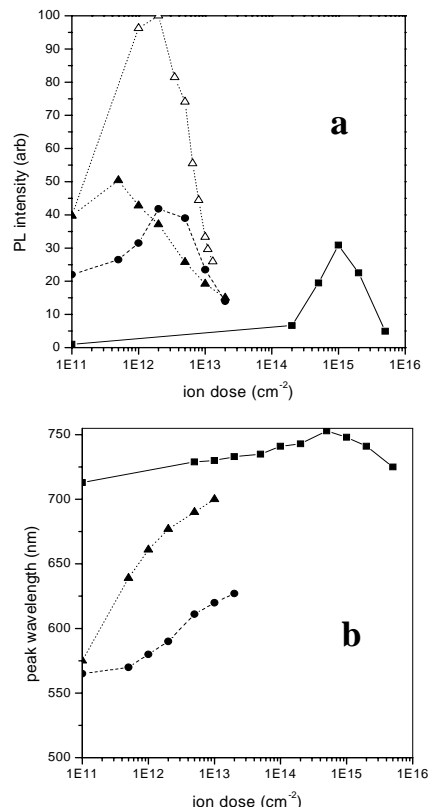


FIGURE 3. (a) Measured PL intensity and (b) peak wavelength emission as a function of dose, for low ($0.02 \Omega\cdot\text{cm}$, solid line) and moderate resistivity ($0.3 \Omega\cdot\text{cm}$, dotted line) and ($3 \Omega\cdot\text{cm}$, dashed line) *p*-type silicon wafers.

A demonstration of this different behaviour is shown in Fig. 4a,b. In low resistivity *p*-type silicon the irradiated dragon produces bright, red PL compared with the faint unirradiated background. In moderate resistivity silicon bright, orange/red PL is produced from the dragon whereas the background produces green PL of a similar intensity. In Fig. 4c,d a range of doses have been irradiated in a continuous distribution in moderate resistivity silicon, producing a gradual change in PL emission wavelength. In Fig. 4c a circular region was irradiated with a dose which increased linearly towards the centre, resulting in a gradual PL red-shift. The tapered region in Fig. 4d was produced by a gradually increased irradiation dose from right to left, again resulting in a gradual PL red-shift.

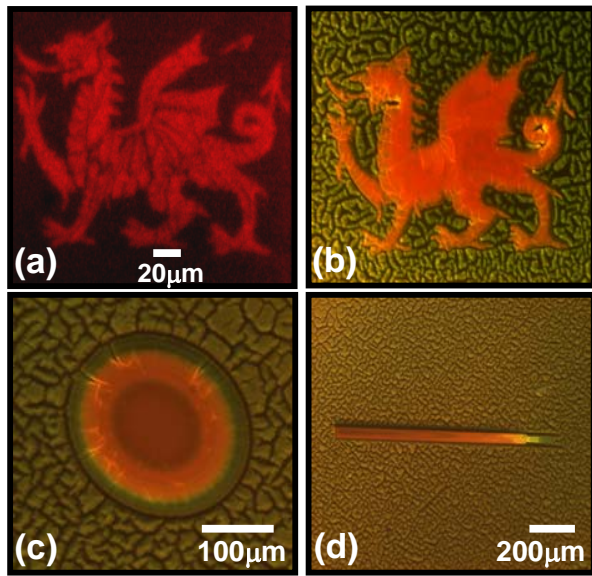


FIGURE 4. Photoluminescence images of dragons formed by irradiating a p-type (a) 0.02 Ω .cm wafer, (b) 3 Ω .cm wafer. (c) Concentric ring pattern in a 3 Ω .cm wafer formed by linearly increasing the dose from the outer edge to the centre. (d) Colour bar showing a gradual wavelength red-shift as the dose increases from the right to the left in a 3 Ω .cm wafer.

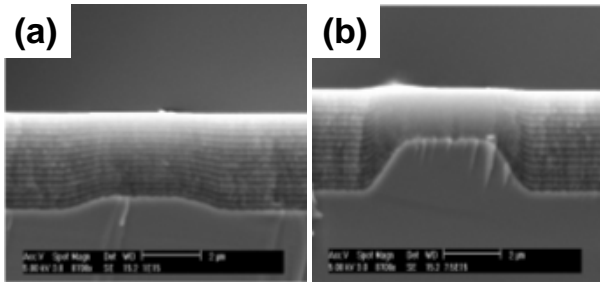


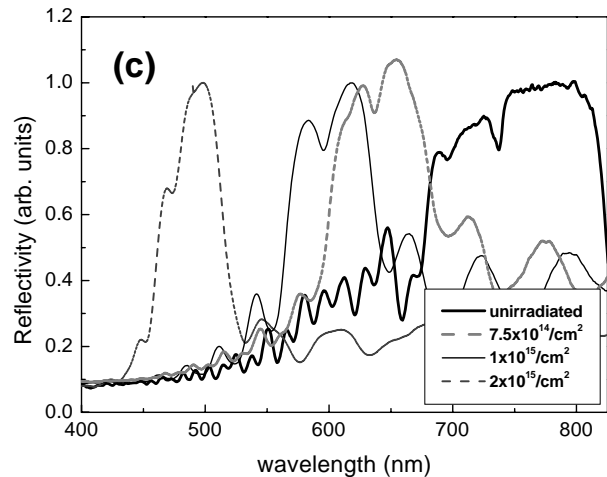
FIGURE 5. SEMs of lines irradiated in a 0.02 Ω .cm wafer with doses of (a) $1 \times 10^{15}/\text{cm}^2$, (b) $7.5 \times 10^{15}/\text{cm}^2$. The irradiated lines (locations shown by the arrow) were 2 mm long and 2 μm wide. (c) Reflectivity spectra of MCs fabricated with different proton doses in the same material. The height of each spectra is normalized to a maximum of 1.0.

DISTRIBUTED BRAGG REFLECTORS

Fig. 5a,b show SEMs of a sample in which lines were irradiated with different doses in a $1 \times 1 \text{ cm}^2$ low

resistivity p-type wafer [19]. The wafer was then etched with an alternating high/low current density for 4 seconds per layer, with a total of 15 bilayers formed, then cleaved perpendicular to the line direction for cross-section imaging. The etched layers appear with light/dark contrast, with high porosity (low refractive) regions appearing darker. The etch rate is progressively slowed by a larger irradiation dose, resulting in thinner porous layers which reflect shorter incident wavelengths. The reflectivity spectra in Fig. 5c were recorded from similar Bragg reflectors produced by irradiating $3 \times 3 \text{ mm}^2$ areas with different proton doses. The unirradiated wafer reflects a central wavelength of 740 nm, which is continuously blue-shifted to 490 nm for a proton dose of $2 \times 10^{15}/\text{cm}^2$.

Fig. 6a shows an optical micrograph of a $500 \times 500 \mu\text{m}^2$ region which was irradiated with different overlaid scan patterns, with different doses. The wafer was etched as in Fig. 5 except the etching period for each layer was chosen to give the central wavelength of 850 nm in the unirradiated regions. Each dose produces a different reflected colour when illuminated with white light, with red/orange colours corresponding to areas irradiated with the lowest dose. The potential of this approach to form patterned array of colour pixel and



lines for display applications is shown in Fig. 6b, where vertical lines, each 10 μm wide, were irradiated to form alternating red-green-blue stripes. The lateral resolution in the image is about 1 micron.

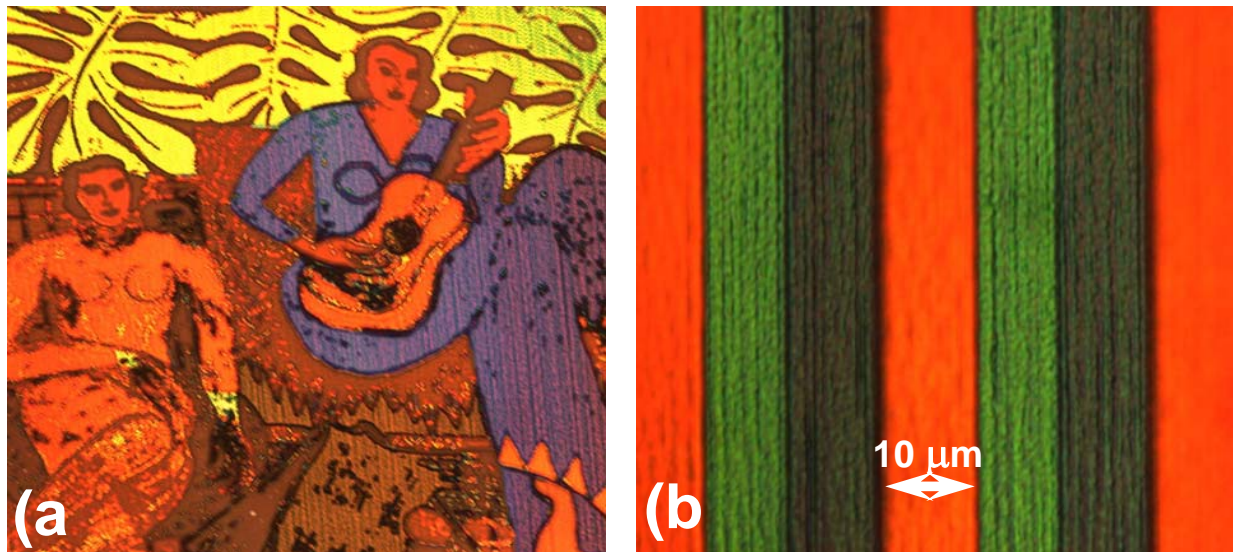


FIGURE 6. Optical reflection images of (a) the painting “La Musique”, by Henri Matisse (1939), created by irradiating a $500 \times 500 \mu\text{m}^2$ area. (b) vertical lines, each $10 \mu\text{m}$ wide, irradiated to form alternating red-green-blue stripes. In each recorded image the sample was illuminated with white light and the reflected light was recorded for 30 seconds using a Nikon Eclipse ME600 microscope with a $\times 10$ objective.

CONCLUSIONS

We have developed the use of high-energy, focused ion beam irradiation to produce patterned porous silicon for a range of different areas of application. In high resistivity silicon, ion irradiation tends to produce patterned pSi with reduced PL intensity but controllably red-shifted. In low resistivity silicon, focused proton beam irradiation can be used to selectively enhance the light emission in the irradiated regions. Tuning of the PL intensity has been obtained by controlling the local resistivity as a function of fluence. If the irradiated wafers are etched with alternating high/low current density, then the reflectivity of the resultant Bragg reflectors is controllably blue-shifted. Focused MeV ion beams in a nuclear microprobe may be used to produce high-aspect ratio, multilevel microstructures in silicon. The feature height of the irradiated structure can be accurately controlled with the fluence of the incident beam, enabling the production of a multilevel structure by multiple fluence exposures in a single irradiation.

REFERENCES

1. A. G. Cullis, L. T. Canham and P. D. J. Calcott, *J. Appl. Phys.* **82**, 909 (1997)
2. S. Ossicini, L. Pavesi and F. Priolo, *Light Emitting Silicon for Microphotonics*, SMTP 194 75 (2003), Springer-Verlag,
3. M. G. Berger, R. Arens-Fischer, M. Kruger, S. Billat, H. Luth, S. Hillbrich, W. Theiß, P. Grosse, *Thin Solid Films*, **297**, 237 (1997)
4. M. Araki, H. Koyama, N. Koshida, *Appl. Phys. Lett.* **69**, 2956 (1996)
5. L. Pavesi, *Riv. Nuovo Cimento* **20**, 1 (1997)
6. S. Nagata, C. Domoto, T. Nishimura, K. Iwameji, *Appl. Phys. Lett.* **72**, 2945 (1998)
7. H. G. Craighead, *Science* **290**, 1532 (2000)
8. S. Y. Lin, J. G. Fleming, D. L. Hetherington, B. K. Smith, R. Biswas, K. M. Ho, M. M. Sigalas, W. Zubrzycki, S. R. Kurtz and Jim Bur, *Nature* **394**, 251 (1998)
9. M. B. H. Breese, D. N. Jamieson, P. J. C. King, *Materials Analysis using a Nuclear Microprobe*, Wiley, New York, **1996**.
10. J. A. van Kan, A. A. Bettiol and F. Watt, *Appl. Phys. Lett.* **83**, 1629 (2003)

11. E. J. Teo, M. B. H Breese, E. P. Tavernier, A. A. Bettiol and F. Watt, M. H. Liu and D. J. Blackwood, *Appl. Phys. Lett.* **84**, 3202 (2004)
12. E. J. Teo, E. P. Tavernier, M. B. H. Breese, A. A. Bettiol, F. Watt *Nucl. Instrum. Methods Phys. Res. B* **222**, 513 (2004)
13. E. J. Teo, M. H. Liu, M. B. H. Breese, E. P. Tavernier, A. A. Bettiol, D. J. Blackwood and F. Watt, *Proceedings of SPIE* **5347**, 264 (2004)
14. J. A. van Kan, A. A. Bettiol and F. Watt, *Nano Letters* **6**, 579 (2006)
15. E. J. Teo, D. Mangaiyarkarasi, M. B. H. Breese, A. A. Bettiol, D. J. Blackwood, *Appl. Phys. Lett.* **85**, 4370 (2004)
16. D. Mangaiyarkarasi, E. J. Teo, M. B. H. Breese, A. A. Bettiol, D. J. Blackwood, *J. Electrochem. Soc.* **152**, D173 (2005)
17. E. J. Teo, M. B. H. Breese, A. A. Bettiol, D. Mangaiyarkarasi, F. J. T. Champeaux, F. Watt, D. J. Blackwood, *Adv. Mater.* **18**, 51 (2006)
18. M. B. H. Breese, F. J. T. Champeaux, E. J. Teo, A. A. Bettiol, D. J. Blackwood, *Phys. Rev. B* **73**, 035428 (2006)
19. D. Mangaiyarkarasi, M. B. H. Breese, Y. S. Ow, C. Vijila, *Applied Physics Letters* **89**, 021910 (2006)